Int j simul model 24 (2025) 1, 5-16
Original scientific paper

EFFECT OF TOPOLOGICAL OPTIMISATION ON THE KINETIC PROPERTIES OF THE KINEMATIC CHAIN

Harl, B.
Faculty of Mechanical Engineering, University of Maribor, Smetanova 17, 2000 Maribor, Slovenia
E-Mail: bostjan.harl@um.si

Abstract
The paper addresses the importance of topology and shape optimisation on improving the performance of a device operating in a mine industry. The process of increasing the stiffness and the value of the first eigenfrequency of the load-carrying structure will be demonstrated. In order to satisfy both objectives simultaneously, two initial optimisation domain models were introduced. The first was the most commonly used optimisation model with full material, while the second was a model with an initial gyroid lattice structure in the optimisation domain. The results obtained by the optimisation of the load-carrying structure were used to analyse the effect of stiffness and eigenfrequency on the four-bar mechanism path of the coupler point and the reduction of the value of the joint forces of the most loaded links.
(Received in September 2024, accepted in January 2025. This paper was with the author 3 weeks for 1 revision.)

Key Words: Topology Optimisation, Shape Optimisation, Eigenfrequency, Kinematic Chain

1. INTRODUCTION

Kinematic chains are devices for varying the type of motion, magnitude of joint forces and torques and are commonly used in heavy industry [1]. Together with the load-carrying structure, kinematic chains form a system that operates under extreme conditions in an industrial sector such as mining [2]. The kinematic chains must provide the best possible guidance and a high degree of rigidity for the entire system, which is very important for a safe workplace. Systems are often subjected to strong vibrations and dynamic loads that can have a negative impact on performance and lifetime [3]. It is also important that systems are designed in a way that eigenfrequency do not come into resonance [4].

Improvements in the performance of systems can be achieved by optimisation methods that lead to an increase in the stiffness and the first eigenfrequency of the load-carrying structure. For such a task, topology optimisation methods are well known in the literature [5]. Topology optimisation is an approach that arranges the material in the optimisation domain. Such an approach leads to crack-free load-carrying structures with longer lifetime and no stress concentrations in the optimised domain [6]. Topology optimisation methods can be roughly divided into homogenisation methods [7], Solid Isotropic Microstructures with Penalisation (SIMP) and the third type of topology optimisation methods that can be traced back under the names Hard-kill or Evolutionary Structural Optimisation (ESO) [8]. The application of these topological methods often results in checkerboard patterns, non-smooth edges, ...

New ideas in the development of topology optimisation methods have brought a level set function into the description of variable boundaries of a structure, supported by mathematical programming methods [9]. This is also the approach used in developing our own topology optimisation programme [10]. During development of the topology optimisation software [11], the function of maximisation of structural lowest eigenfrequency was added to the original function of minimization of structural strain energy.

The results of topological optimisation are non-smooth structure surfaces. Those can be smoothed on the basis of the resulting triangulated surface of the optimised model [12] or, based on the FEM mesh of the topologically optimised model, the shape optimisation can be

performed [13, 14]. For the example considered in this paper, first a topological optimisation of a model has been performed, which was then used for shape optimisation. Shape optimisation is usually less sophisticated from the procedural point of view compared to topological optimisation. Although these problems are still non-linear and non-convex, they are typically rather non-flat problems. Therefore, the optimisation process is usually rather straightforward and monotonic [15]. Such topology and shape optimised structures can be made with casting, moulding or additive manufacturing [16].

The topology optimisation of the load-carrying structure influences the performance of the kinematic chains of the entire system. In the case of kinematic chains, the shape of the path and, consequently, the magnitude of the joint forces are important for proper operation [17]. Systems often contain closed kinematic chains called four-bar mechanism, where the desire is to achieve a specific path of a coupler point, as this is the only way to achieve trouble-free operation of the whole system. The appropriate path design can be achieved by satisfying the condition of minimal nodes displacements of the kinematic chain [18], which can be done by increasing the stiffness of the load-carrying structure. The nodes displacements with other kinetic quantities affect the magnitude of the joint forces.

The outline of this paper is as follows. Section 2 briefly presents the ideas and concepts in topology and shape optimisation as well as the implementation of kinetic analysis of kinematic chains. Section 3 presents the theoretical background used in the shown simulations. Sections 4 and 5 present the model preparation and the interpretation of the simulation results. Fig. 1 shows a schematic flow of the simulation.

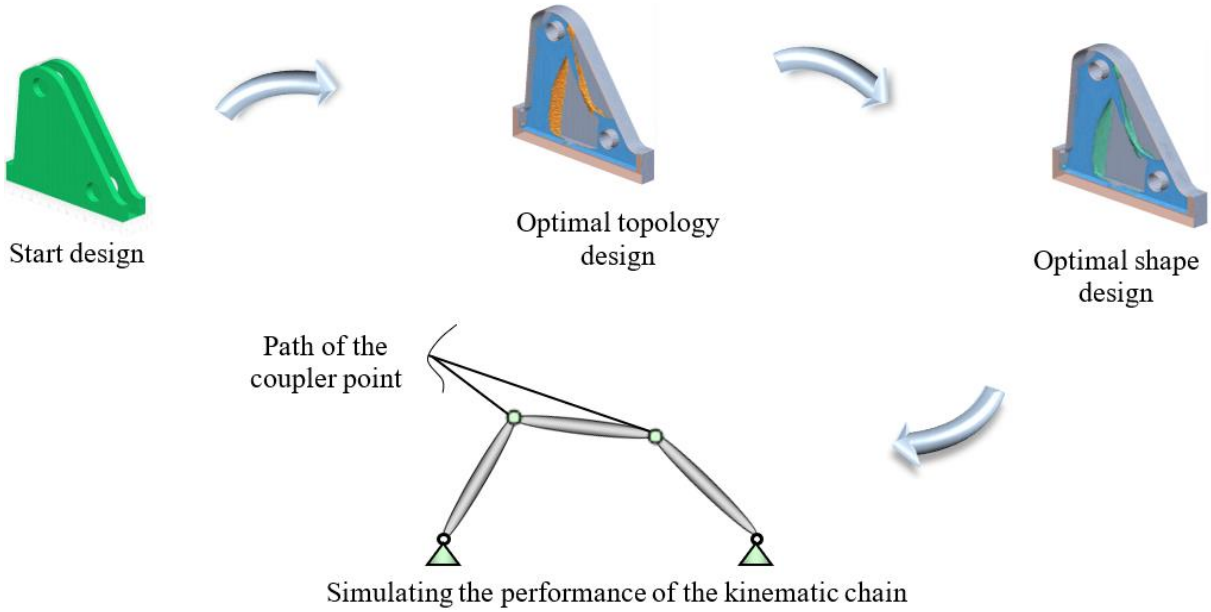

Figure 1: Simulation flow chart.

2. THE THEORETICAL BASIS OF THE SIMULATION

Topology optimisation of structures aims at achieving better static and dynamic properties, eliminating stress concentrations in the optimisation domain, thus giving the structures a prolonged service life. The method is based on:

- obtaining the best models by automated simulation based on FEA,
- removing the material in low stress areas and adding the material in high stress areas.

Normally the topology optimisation problem is mathematically formulated as:

$$\min f(\Gamma),\ V \leq \gamma V_{start} \tag{1}$$

where $f(\Gamma)$ is a function of the strain energy of the structure, V denotes the structural optimisation volume, V_{start} is the initial optimisation volume and γ is a coefficient between 0 and 1. In addition to increasing the stiffness of the system structure, a goal is also to increase the value of the first eigenfrequency. Therefore, the basic topological optimisation problem was upgraded and another objective function was added to the optimisation task. Firstly, it was necessary to calculate eigenfrequency of the system using the Eq. (2):

$$\det(\boldsymbol{K} - \boldsymbol{\lambda M}) = \boldsymbol{0} \tag{2}$$

where $\boldsymbol{K}$ is stiffness matrix, $\boldsymbol{M}$ mass matrix and $\boldsymbol{\lambda}$ eigenvalues related to eigenfrequency. The new optimisation problem thus covered two individual objectives: minimisation of the strain energy of the structure and maximisation of the lowest eigenfrequency of the structure. These two objectives can be considered individually or together. In the latter case, the two objectives are combined into a single one, where the weighting factors ζ and η define the relative importance of one objective compared to the other.

$$\min(\zeta f(\Gamma) + \eta f(\lambda)), V \leq \gamma V_{start} \tag{3}$$

The process of topologically maximising the value of the lowest eigenfrequency in a structure is a relatively stable process, but only until the lowest and second lowest frequencies meet [19]. As the optimisation continues, the lowest eigenfrequency increases while the second lowest eigenfrequency tends to decrease, and the optimisation process must be stopped, as shown in Fig. 2.

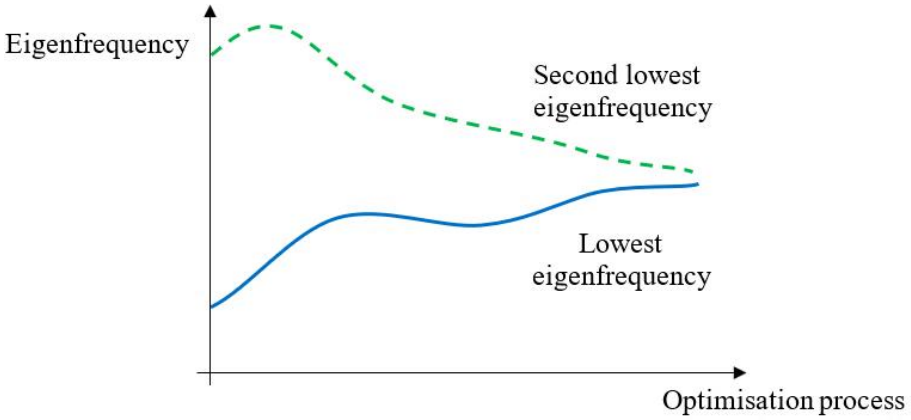

Figure 2: Optimisation of eigenfrequency.

Due to the lack of knowledge of the exact load or whole boundary conditions of the system, the initial optimisation domains are often modelled by lattice structures to limit the allowable topological space and to impose a certain material distribution [20]. For this purpose, the gyroid cell structure is used in this paper, shown in Fig. 3. It should be emphasized that topological optimisation is the best from the mathematical point of view, if the optimisation starts from a full structure (optimisation domain is full). However, this optimum may also have limited applicability in real engineering applications. Topological optimisation of the solid model adapts the structure as much as possible to the boundary conditions, i.e., loads and supports. Meaning that the resulting solution is excellent for the selected boundary conditions, but may be sensitive to very small changes. In practice, the desire is to obtain a reliable solution (achieved by optimised lattice structures), which in reality is more difficult to produce and more costly.

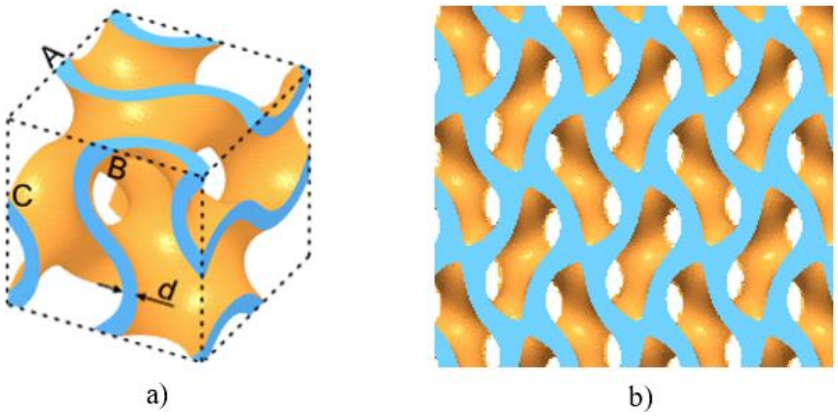

Figure 3: a) Gyroid cell size $A \times B \times C$ and thickness d [11], b) Gyroid structure.

Geometric smoothing of surfaces in this paper is performed by shape optimisation. This optimisation is designed to improve the surfaces obtained by topological optimisation. The goal is to improve the smoothness of the newly obtained surfaces by moving the FE nodes to more appropriate positions. The surface nodes are moved so that the element and node normal are as parallel as possible, as illustrated in Fig. 4.

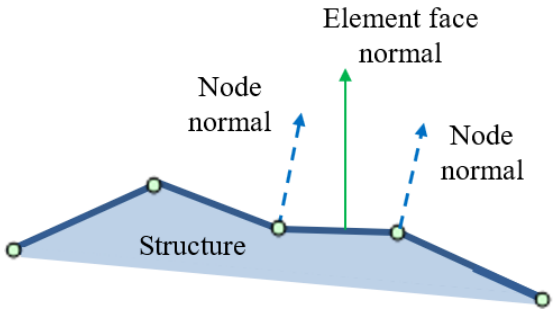

Figure 4: Shape optimisation.

The result of the design optimisation of the load-carrying structure is used to study and simulate the kinematic chain operation. The equations of the desired kinematic chain path (four-bar coupler point) can be written analytically. The local vector $\boldsymbol{p}$ of the observation point depends on the length of the links l_i of the kinematic chain, the change of the angle as a function of time $\varphi(t)$ and the tolerances of the links Δl_i:

$$\boldsymbol{p} = \boldsymbol{p}(l_i, \varphi(t), \Delta l_i) \quad i = 1, \dots n \tag{4}$$

where n is the number of links of the kinematic chain.

After the kinematic analysis, where the velocity vectors $\boldsymbol{v}_i$ and the acceleration vectors $\boldsymbol{a}_i$ in addition to the vectors $\boldsymbol{r}_i$ were calculated, a kinetic analysis of the kinematic chain was made. To calculate the kinetic quantities, especially joint reaction forces $\boldsymbol{F}_i$, a system of equations can be written as:

$$\sum_{i=1}^{n} \boldsymbol{F}_i + \boldsymbol{F}_{ext_i} + \boldsymbol{F}_{g_i} = m_i \mathbf{a}_i, \sum_{i=1}^{n} \mathbf{s}_i \times \boldsymbol{F}_i + \boldsymbol{M}_i = J_i \boldsymbol{\alpha}_i \tag{5}$$

where $\boldsymbol{F}_{ext_i}$ is an external force acting on the centre of gravity of the link, $\boldsymbol{F}_{g_i}$ is the gravity force of the link, m_i is the mass of the i^{th} link, $\boldsymbol{a}_i$ is the acceleration of its centre of gravity, $\boldsymbol{s}_i$ is vector from the centre of gravity of the i^{th} link to the points where the joint forces is imposed, J_i is its inertial mass moment, $\boldsymbol{\alpha}_i$ is its angular acceleration vector and $\boldsymbol{M}_i$ are the moments in the joints of the link, shown in Fig. 5.

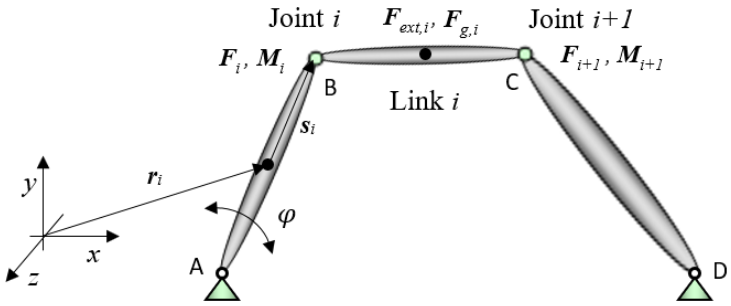

Figure 5: Model of the kinematic chain (four-bar mechanism).

3. DEFINITION OF THE OPTIMISATION MODEL

The system considered below is used for protection of workers and equipment in a coal mine [21] and consists of a load-carrying structure and kinematic chains. The kinematic chain consists of two four-bar mechanisms, the leading EFCD and the driven ABCD, shown in Fig. 6. The system considered is designed in a way that the kinematic chains allow minimum vertical deflection of the upper platform of the structure from the ideal vertical path and give lateral stability to the system. The performance of the system has been affected by deficiencies in the load-carrying structure [22], where high forces at the joints of the kinematic chains and the effect of vibrations have led to malfunctions and damage to the system [23]. It has been decided to investigate how topological optimisation could be used to improve the load-carrying structure in a way to provide more optimal path of the coupler point of four-bar mechanism ABCD of the kinematic chain and consequently reduce the joint forces in the most stressed joints of the kinematic chains.

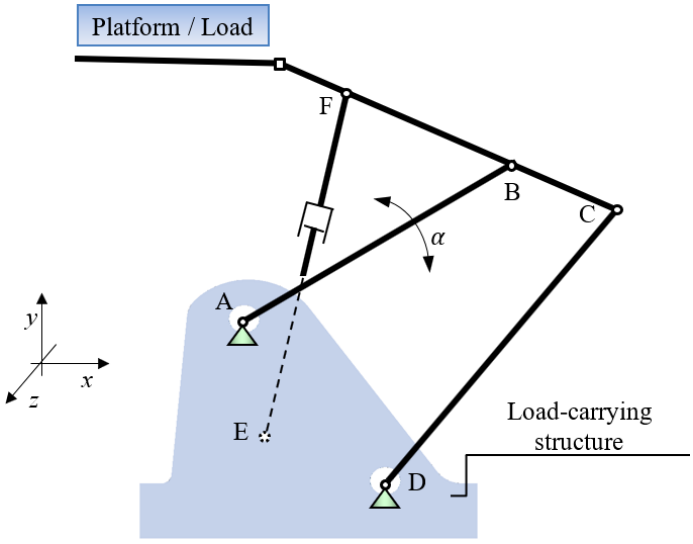

Figure 6: System with load-carrying structure and two four-bar mechanisms.

The load-carrying structure was modelled with PTC® Creo® software [24]. A FEA model was prepared containing approximately 2 million FE (linear tetrahedron). The structure is made out of material S355 JO, with mechanical properties $E = 2 \cdot 10^5$ MPa and $\nu = 0.27$.

The topological optimisation was performed with our own optimisation software CAESS ProTOp [11]. When preparing a topological model for optimisation, it is first necessary to determine the volume regions where material will be added or subtracted (free domain – blue) and the fixed regions where it will remain unchanged (grey), shown in Fig. 7 a. The next step is to define the boundary conditions such as loads and structural supports of the model, shown in Fig. 7 b.

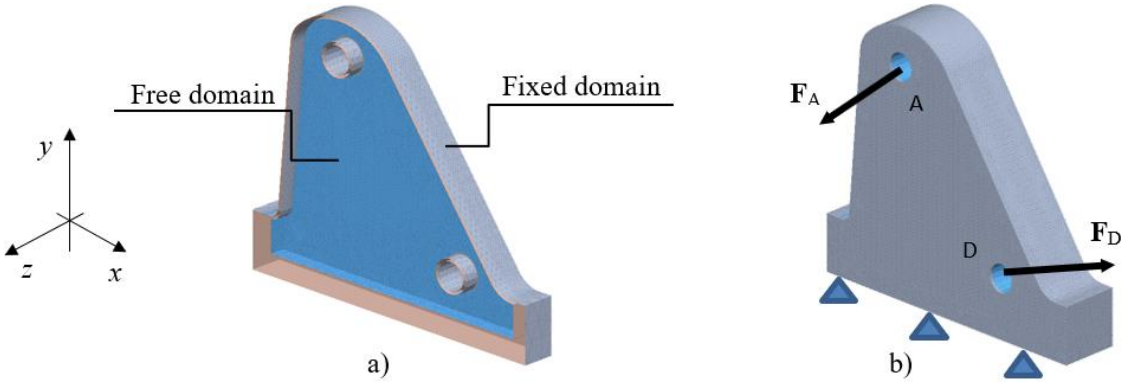

Figure 7: Load-carrying structure: a) Volume regions, b) Boundary conditions.

The loads on the load-carrying structure at joints A and D (Fig. 7 b) were calculated based on the operation of a kinematic chain consisting of two four-bar mechanisms EFCD and ABCD. The data preparation is based on the assumption that the four-bar mechanism ABCD is able to move in a way that the angle α is in the interval between 76.8° and 94.8° with respect to the horizontal x-axis (Fig. 6). The device is loaded with earth ore, which may result in a maximum force magnitude in the hydraulic actuator arm EF of 800 kN. Based on the maximum load and the friction coefficient between the load-carrying structure and earth ore $\mu = 0.3$, the magnitudes of the joint forces in links A and D have been calculated for the cases of angles 76.8° and $\alpha_{i+1} = \alpha_1 + i \cdot 3°$, $i = 1, 2, \ldots, 6$ (Table I). The initial lengths of the arms of the kinematic chain are $\overline{AB} = 1360$ mm, $\overline{BC} = 382$ mm, $\overline{AD} = 674$ mm and the masses are $m_1 = 230$ kg, $m_2 = 1795$ kg and $m_3 = 485$ kg.

Table I: Loads in the joints of a load-carrying structure.

	Joint A		**Joint D**	
Set	$\boldsymbol{F_x}$ [kN]	$\boldsymbol{F_y}$ [kN]	$\boldsymbol{F_x}$ [kN]	$\boldsymbol{F_y}$ [kN]
1	- 357.14	- 433.03	746.51	- 354.88
2	- 332.50	- 405.38	730.39	- 330.25
3	- 308.92	- 381.88	716.68	- 306.67
4	- 285.64	- 362.10	705.25	- 283.39
5	- 261.67	- 345.83	696.40	- 259.42
6	- 235.88	- 333.09	690.42	- 233.63
7	- 206.73	- 324.23	687.55	- 204.47

Due to the low inclination of the upper platform of the system during operation (Fig. 6), the lateral force in the positive and negative direction of the z-axis was considered. Its value was $F_l = 10$ kN. In the topological optimisation, it is necessary to define all possible load cases (LC) containing the data of the structural supports and loads. When the structure is subjected to several load cases, all of them have to be considered in the optimisation problem, however, computationally each one has to be treated separately. In our case, 14 load cases have been defined $LC_i = Set_j \pm F_l$ $(i = 1, \ldots, 14; j = 1, \ldots, 7)$.

Topology optimisation does not lead to a single optimal solution for the structure. In order to show the importance of defining the initial parameters of a topology problem and their influence on the solution, several examples were made. Firstly, three different initial cases of the optimisation region (OR) were chosen:

- OR1 – empty, meaning that material is inserted and redistributed during the optimisation process,

- OR2 – full, resulting in material being largely removed and redistributed during the optimisation process,
- OR3 – a lattice gyroid cell structure, which means that a certain distribution of material has been imposed.

Secondly, three different objective tasks (OT) were chosen:

- OT1 – the optimisation is set to 100 % stiffness influence and no influence of the optimisation of the first eigenfrequency value,
- OT2 – the optimisation is set to 50 % stiffness influence and 50 % first eigenfrequency value influence,
- OT3 – the optimisation is set to 100 % influence of the increase of the eigenfrequency value.

By combining the cases of optimisation regions OR and objective tasks OT, 9 combinations of topology tasks T_i, $i = 1, \ldots, 9$ were made, listed in Table II.

Table II: Topology tasks.

Case	Optimisation region	Objective tasks
T1	OR1	OT1
T2	OR1	OT2
T3	OR1	OT3
T4	OR2	OT1
T5	OR2	OT2
T6	OR2	OT3
T7	OR3	OT1
T8	OR3	OT2
T9	OR3	OT3

The obtained topological optimisation results were compared with the initial load-carrying structure and two non-optimised structures, where longitudinal and vertical reinforcement ribs were added intuitively.

4. RESULTS OF THE SIMULATION

In order to assess the performance of the topology optimisation, the initial displacement values (Fig. 8 b), the first eigenfrequency values and the stress values (Fig. 8 c) for the initial load-carrying structure (Fig. 8 a) were calculated. The stress nowhere excided 300 MPa and was therefore not considered further. For all cases made, the values of displacements and natural frequencies are given in Table III.

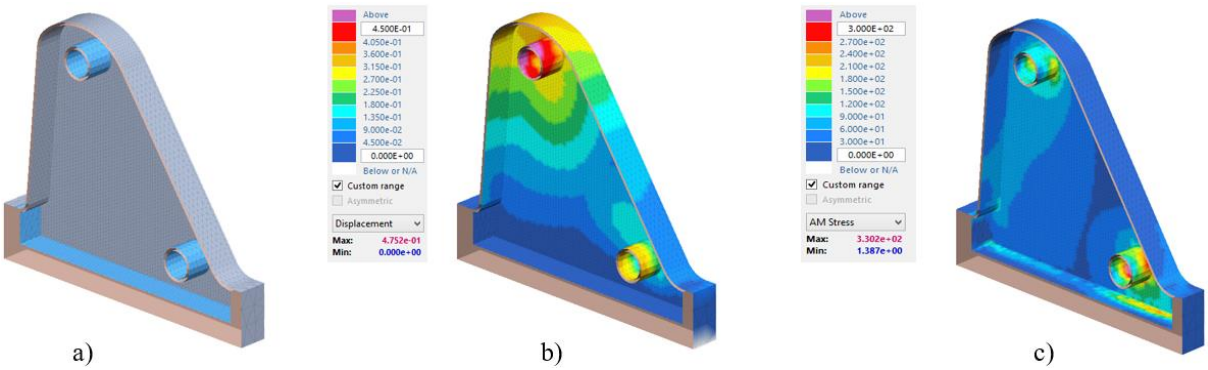

Figure 8: Initial load-carrying structure: a) Design, b) Displacement, c) Stress.

For comparison with the topology optimisation results, two structures with differently positioned ribs were made. The displacement values for both cases are given in Fig. 9.

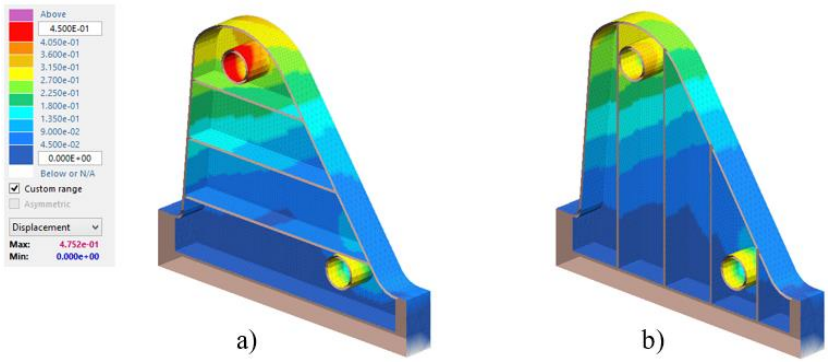

Figure 9: Load-carrying structure: a) Horizontal ribs, b) Longitudinal ribs.

In Figs. 10 to 12, the results of the topological optimisation for the cases T1 – T9 together with their displacement values are shown. Fig. 10 shows the optimised models with empty initial domain T1 – T3.

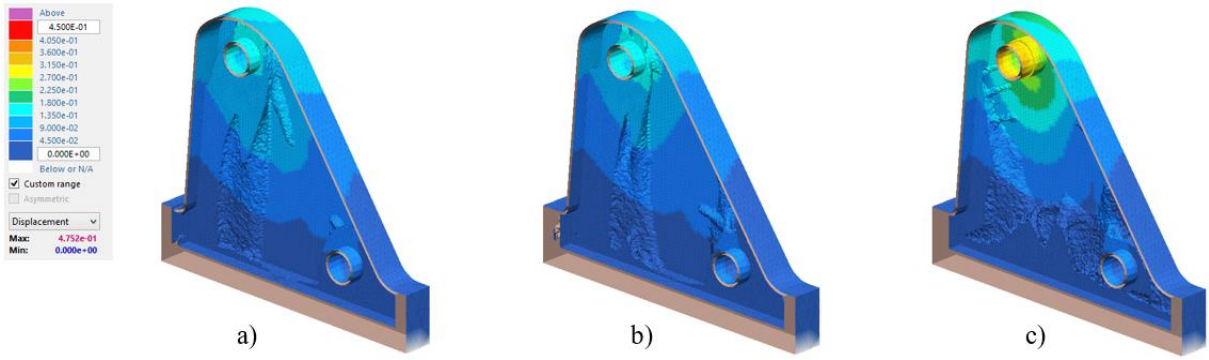

Figure 10: Optimal load-carrying structure: a) T1, b) T2, c) T3.

Fig. 11 shows the optimised models with the full initial domain T4 – T6.

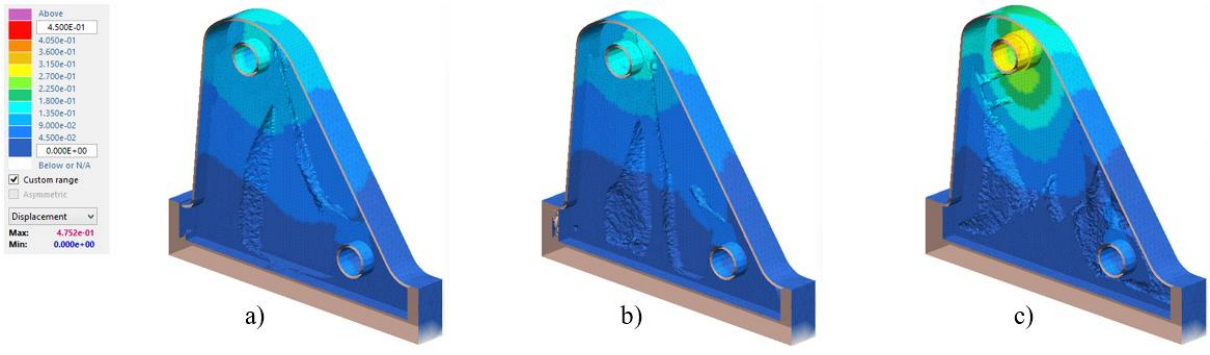

Figure 11: Optimal load-carrying structure: a) T4, b) T5, c) T6.

Fig. 12 shows the optimised models with the gyroid lattice structure, T7 – T9.

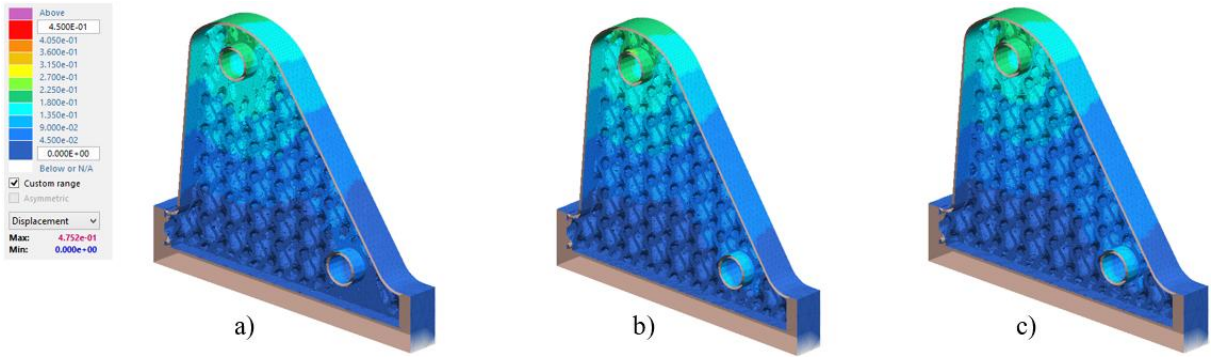

Figure 12: Optimal load-carrying structure: a) T7, b) T8, c) T9.

For optimisation cases T1 – T9 shape optimisation was also performed. Fig. 13 shows only the shape optimisation of models T4 – T6, which, according to the results in Table III, proved to be the most suitable for manufacturing with AM technology.

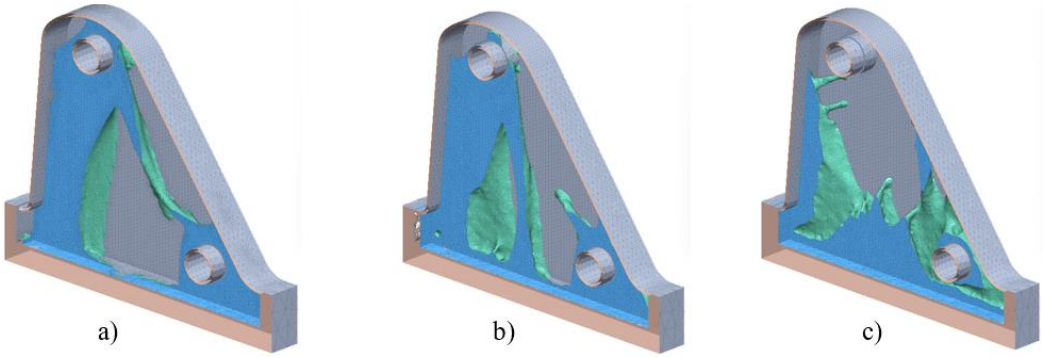

Figure 13: Topologically and shape optimised load-carrying structure: a) T4, b) T5, c) T6.

Shown in Table III are the results for all previously mentioned models (values of displacements and the lowest eigenfrequencies).

Table III: The value of the displacements and the lowest eigenfrequency.

Case		**Max displacement of joint A** [mm]	**Lowest eigenfrequency** [Hz]
1	Initial structure	0.472	245
2	Horizontal ribs	0.429	258
3	Longitudinal ribs	0.337	311
4	T1	0.161	243
5	T2	0.174	294
6	T3	0.341	330
7	T4	0.160	245
8	T5	0.174	294
9	T6	0.344	330
10	T7	0.210	236
11	T8	0.270	238
12	T9	0.224	240

Table III shows that the displacement in joint A was reduced the most in the case of optimisation task T4. The value of the first eigenfrequency has increased the most in the case T6. However, if we want to consider the average of both values, the best result was achieved

by model T8, with lattice gyroid cell structure. The results show that topological optimisation cannot achieve the maximal increase of the first eigenfrequency and the maximal reduction of displacements at the same time. Both can only be improved. Fig. 14 shows the normalized results from the table in a bar chart.

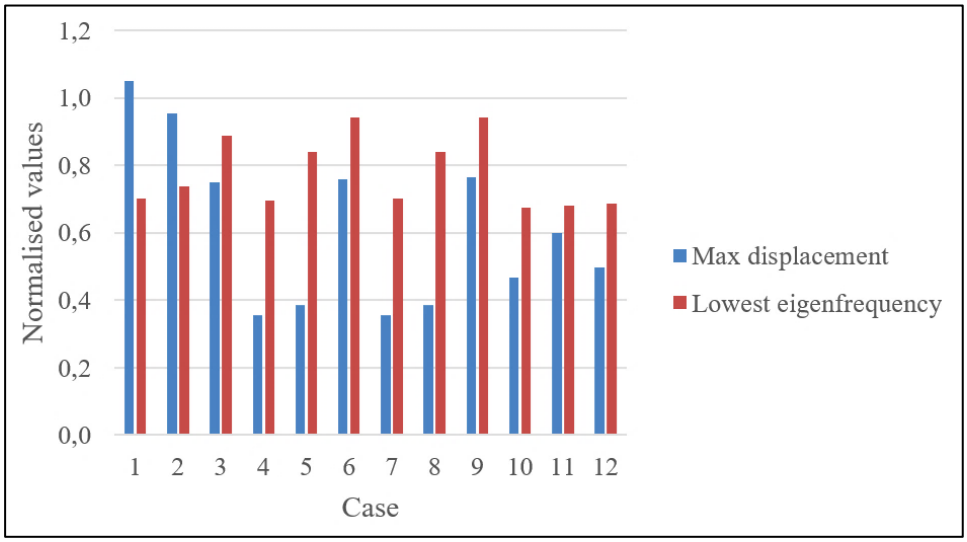

Figure 14: Normalized displacements and lowest eigenfrequency.

The results obtained from the optimisation were used to calculate the path of the system platform in Fig. 6. The calculation was performed for the case with initial structure and case T4. Fig. 15 shows that the motion path of the structure in the maximum position in case T4 is on average shifted towards the desired ideal vertical line of the system.

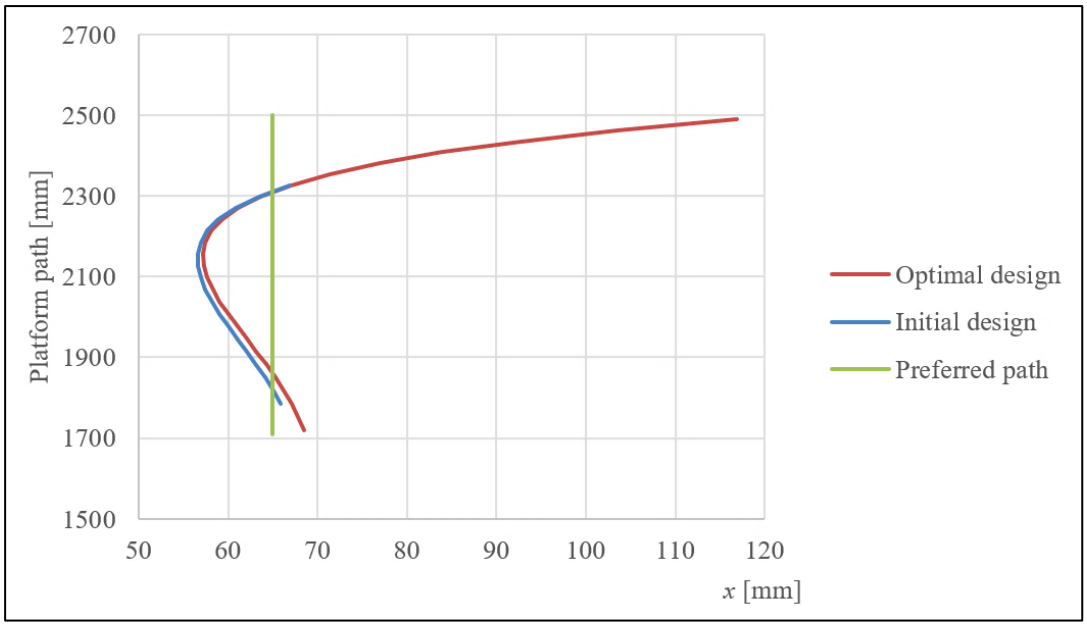

Figure 15: Path of the system platform.

The forces at the most loaded joints (A, D) have also been calculated for the same cases (case with initial structure and case T4) and are shown in Fig. 16. Results show that the joint forces were reduced in almost all positions of the platform, confirming the success of the optimisation.

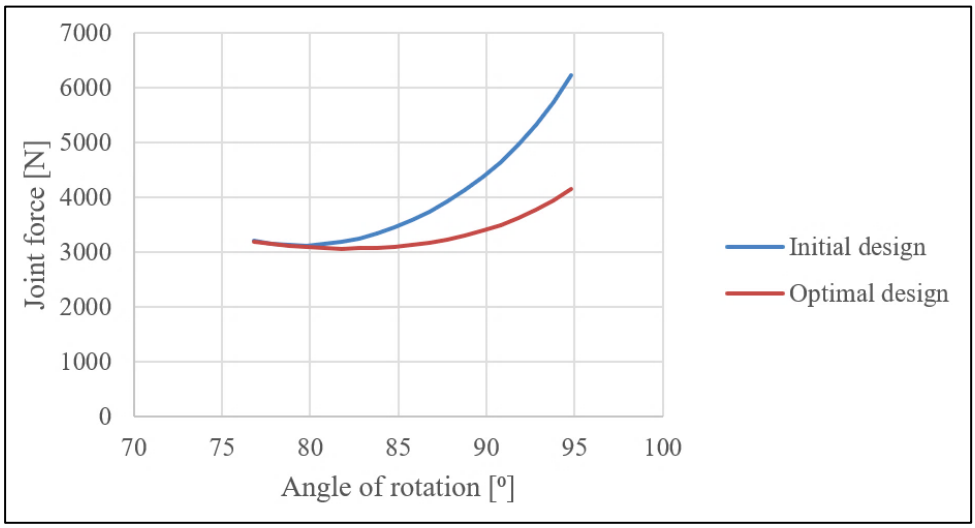

Figure 16: The joint forces.

5. CONCLUSION

In this paper the implementation of a set of design optimisations and their impact on the kinematic and kinetic properties of the kinematic chain is shown. Modern optimisation procedures adapt structures to certain boundary conditions, which must therefore be carefully prepared. The results showed that the improvement was successfully implemented, but not simultaneously increasing the first eigenfrequency and reducing the displacements. On average, the lattice gyroid structure performed best, however it would be expensive and difficult to implement in practice.

Lattice structures have been proven useful in engineering practice. Difficulties arise in manufacturing. Further research is aimed at developing new shapes that might be easier to manufacture as well as developing topological methods to mimic biomimetic structures.

ACKNOWLEDGMENT

The research was supported by grants from the Slovenian Research and Innovation Agency P2-0137 “Numerical and experimental analysis of nonlinear mechanical systems”.

REFERENCES

[1] Rudall, B. H. (1997). Reports & Surveys: Development programmes for business automation, *Robotica*, Vol. 15, No. 2, 199-206, doi:10.1017/S0263574797000210

[2] Chai, G. F.; Xia, Y. Z. (2023). Multi-robot path optimization and simulation for multi-route inspection in manufacturing, *International Journal of Simulation Modelling*, Vol. 22, No. 1, 121-132, doi:10.2507/IJSIMM22-1-CO1

[3] Ma, H. W.; Xue, L. M.; Wang, C. W. (2024). Cutting vibration response of a shield-type tunnelling robot system, *International Journal of Simulation Modelling*, Vol. 23, No. 4, 656-667, doi:10.2507/IJSIMM23-4-705

[4] Drosopoulos, G. A.; Gogos, C.; Foutsitzi, G. (2023). Multi-objective optimization for maximum fundamental frequency and minimum cost of hybrid graphene/fibre-reinforced nanocomposite laminates, *Structures*, Vol. 54, 1593-1607, doi:10.1016/j.istruc.2023.05.118

[5] Rozvany, G. I. N. (2009). A critical review of established methods of structural topology optimization, *Structural and Multidisciplinary Optimization*, Vol. 37, 217-237, doi:10.1007/s00158-007-0217-0

[6] Harl, B.; Predan, J.; Gubeljak, N.; Kegl, M. (2017). On configuration-based optimal design of load-carrying lightweight parts, *International Journal of Simulation Modelling*, Vol. 16, No. 2, 219-228, doi:10.2507/IJSIMM16(2)3.369
[7] Huang, X.; Xie, Y. M. (2010). *Evolutionary Topology Optimization of Continuum Structures: Methods and Applications*, John Wiley & Sons, New York
[8] Bendsøe, M. P.; Kikuchi, N. (1988). Generating optimal topologies in structural design using a homogenization method, *Computer Methods in Applied Mechanics and Engineering*, Vol. 71, No. 2, 197-224, doi:10.1016/0045-7825(88)90086-2
[9] Wang, M. Y.; Wang, X.; Guo, D. (2003). A level set method for structural topology optimization, *Computer Methods in Applied Mechanics and Engineering*, Vol. 192, Nos. 1-2, 227-246, doi:10.1016/S0045-7825(02)00559-5
[10] Harl, B.; Kegl, M. (2022). Topology optimization course for mechanical engineering students, *International Journal of Mechanical Engineering Education*, Vol. 50, No. 2, 364-388, doi:10.1177/0306419020967883
[11] CAESS – Center for Advanced Engineering Software and Simulations. CAESS ProTOp Software, from *https://caess.eu/*, accessed on 13-09-2024
[12] Jones, N. L.; Wright, S. G. (1991). Algorithm for smoothing triangulated surfaces, *Journal of Computing in Civil Engineering*, Vol. 5, No. 1, 85-102, doi:10.1061/(ASCE)0887-3801(1991)5:1(85)
[13] Seo, Y.-D.; Kim, H.-J.; Youn, S.-K. (2010). Shape optimization and its extension to topological design based on isogeometric analysis, *International Journal of Solids and Structures*, Vol. 47, Nos. 11-12, 1618-1640, doi:10.1016/j.ijsolstr.2010.03.004
[14] Ding, Y. (1986). Shape optimization of structures: a literature survey, *Computers & Structures*, Vol. 24, No. 6, 985-1004, doi:10.1016/0045-7949(86)90307-x
[15] Plotnikov, P. I.; Sokolowski, J. (2023). Geometric aspects of shape optimization, *The Journal of Geometric Analysis*, Vol. 33, Paper 206, 57 pages, doi:10.1007/s12220-023-01252-7
[16] Zhu, J.; Zhou, H.; Wang, C.; Zhou, L.; Yuan, S.; Zhang, W. (2021). A review of topology optimization for additive manufacturing: status and challenges, *Chinese Journal of Aeronautics*, Vol. 34, No. 1, 91-110, doi:10.1016/j.cja.2020.09.020
[17] Vohar, B.; Gotlih, K.; Flašker, J. (2003). Optimal kinematic design of a link-drive mechanism with prescribed velocity characteristics, *Proceedings in Applied Mathematics and Mechanics*, Vol. 3, No. 1, 527-528, doi:10.1002/pamm.200310533
[18] Koivo, A. J. (1989). *Fundamentals for Control of Robotic Manipulators*, *Wiley*, New York
[19] Braibant, V.; Fleury, C. (1985). An approximation-concepts approach to shape optimal design, *Computer Methods in Applied Mechanics and Engineering*, Vol. 53, No. 2, 119-148, doi:10.1016/0045-7825(85)90002-7
[20] Kegl, M.; Harl, B.; Gubeljak, N.; Predan, J. (2023). Implementacija in uporaba giroidne celice pri optimizaciji topologije (Implementation and usage of a gyroid cell in topology optimization), *Zbornik del Kuhljevi dnevi 2023 (Proceedings)*, 99-108 (in Slovene)
[21] Grm, V. (1992). *Optimalna sinteza 4-zgibnega mehanizma (Optimal synthesis of four-bar mechanism)*, Master Thesis, Technical Faculty, Mechanical Engineering, Maribor (in Slovene)
[22] Mi, C.; Hai, Y.; Wu, F.; Luo, L.; Chen, Z.; Fan, Y.; Kang, D. (2023). Fuzzy multi-objectives topology optimization of slider pallet in the picking machine of camellia fruit, *Technical Gazette*, Vol. 30, No. 5, 1627-1634, doi:10.17559/TV-20230111000218
[23] Tanriver, K.; Ay, M. (2023). Experimental, software and topological optimization study of unpredictable forces in bolted connections, *Technical Gazette*, Vol. 30, No. 4, 1175-1184, doi:10.17559/TV-20221113121639
[24] PTC. CREO Software, from *https://www.ptc.com/en/products/creo*, accessed on 13-09-2024